

Exploration of Innovative Radar Sensing Schemes for Subsurface Object Detection

Kevin O'Neill

U.S. Army Cold Regions Research and Engineering Laboratory (CRREL)
72 Lyme Rd Hanover, NH 03755 USA
603-646-4312 koneill@crrel.usace.army.mil

The problem of abandoned landmines and unexploded ordnance is particularly acute when these objects are near the surface, so that their radar returns cannot easily be separated from the ground surface response. To address this, we pursue simulations here designed to test methods of sensor deployment and data processing that exploit angular, positional, and frequency diversity for detection of metallic targets that are on the order of the subsurface wavelength in size. Rigorous 2-D computations were performed and results processed for the angular correlation function (ACF) approach, in which one performs a coherent average of received signals from two incidence and observation angles. Simulations pursue the behavior of the ACF under realistic ground roughness and moisture content, target geometry, and highest practical resolution GPR frequencies. To achieve an expanded ensemble of cases, given a single subject ground surface, we average both over frequencies and overlapping incident beam locations.

INTRODUCTION

The investigations discussed here are part of a larger study in which measurements and simulations are pursued to test innovations in sensing strategy for detection of buried objects. A principal motivation is to improve methods for detecting abandoned landmines or unexploded ordnance. These objects pose an enormously widespread and urgent problem worldwide, and also put extraordinary burdens on subsurface sensing methods. This is partial because the criteria applied must

be extremely strict, requiring an absolute minimum of both false positive and false negative judgments as to the presence of a target sought. This is particularly challenging in as much as the targets of interest typically reside in randomized environments. Simply increasing the sensitivity of sensors tends to inundate the record with irrelevant clutter. One must pursue creative sensing strategies, by which we mean the totality of sensor configuration, combination, deployment, and data processing methods.

The nature of the problem is illustrated in Figure 1, which shows bistatic results from 2-D numerical solutions for radar reflection from metallic targets embedded in a moist soil with randomly rough surface. The two targets are approximately the same size, one elliptically shaped and the other having a mine-like geometrical cross section (Figure 2). Radar cross section values are shown, arbitrarily but consistently scaled, in negative scattering directions, i.e. back into the quadrant occupied by the transmitter. For these results from a single frequency, incidence angle, and beam position, one sees that relative visibility of the subsurface target depends very much on which target one considers and which observation angle he chooses.

We must pool data to ascertain ways in which any of a variety of targets will stand out, reliably and over a broad range of angular and environmental conditions. Because our targets of concern are quite localized, one's options are limited for achieving an ensemble of sensor data for processing. We proceed by defining a particular scene (Figure 2) and solving for the scattered response over a broad frequency band, variety of incidence and observation angles, and beam position com-

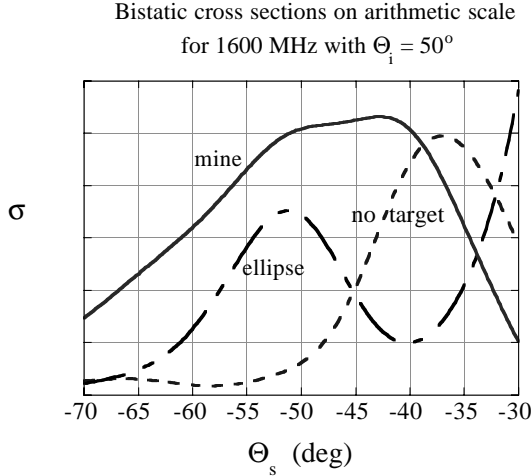


Figure 1. Bistatic radar cross sections at 1600 MHz for rough ground with and without buried target.

binations. We then investigate the behavior of ACF processing schemes when applied to that data.

SIMULATION AND PROCESSING APPROACH

The example target (Fig. 2) is 10 cm high, 22 cm wide at the base, buried with its top 5 cm below the mean surface. We treat only horizontal polarization here (E field into the page). The taper of the beam is illustrated by the E field solution magnitudes shown for to-

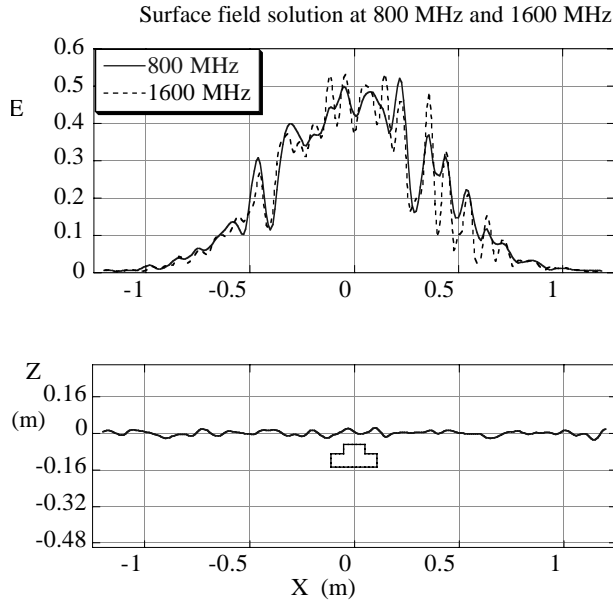


Figure 2. Example target and surface geometry, with ground surface field solution.

tal field along the soil surface. Environmental randomness is expressed through the rough soil surface, which is otherwise homogeneous. The real part of the soil dielectric constant is 9, typical of a moist soil, and its electrical conductivity is 10^{-3} S/m.

The random surface is generated by selecting a parent distribution Fourier transform $Z(K)$ of its height profile, corresponding to a power spectrum $W(K)$ in the form of a Rayleigh distribution.

$$W(K) = \frac{\pi \ell^2 h^2}{2} |K| \exp\left(\frac{-\pi K^2 \ell^2}{2}\right) \quad (1)$$

where h is the root mean square height and ℓ the correlation length. This suppresses low frequency surface shape components and produces many relatively small bumps, as shown. We choose $Z(K)$ proportional to

$\sqrt{W(K)}$ for each K , but then randomize the phase of the component. This produces an ensemble in which each member surface is different but has the same specified h and ℓ equal here to 1 cm and 3 cm respectively. The E field is obtained from numerical solution of an integral equation in the manner of [1], for each electromagnetic frequency, beam position, and surface.

To achieve positional diversity we shift the beam from side to side over five positions: centered over the target, and centered over points ± 25 cm and ± 50 cm from there. Thus the target remains at least generally within the main beam, and with each shift of the beam we change the sample of the surface by a significant amount. Examination of amplitude and phase of backscatter suggests that this is the best we can do with these surface parameter/ radar wavelength relations. Larger shifts would take us away from the target. Scattering data are pooled from nine frequencies equally spaced between 800 MHz and 1600 MHz. This appears optimal from the point of the view of the angular correlation study over this band. That is, a coarser frequency division shows angular correlation effects poorly; a finer division produces samples that are less independent, thus bringing no improvement. Altogether, with five shifts and nine frequencies, we achieve an ensemble of 45 cases for each surface surveyed, over a total ensemble with 25 such surfaces.

Recent work suggests that angular correlation function analysis (ACF) may succeed in suppressing scattered signal clutter from random surface irregularities, relative to the effect of the target [2]. One computes the complex product of fields scattered in directions Θ_{s1} and Θ_{s2} produced by incident waves from directions Θ_{i1} and Θ_{i2} , respectively.

$$ACF = \left\langle E(\Theta_{s1}, \Theta_{i1}) E^*(\Theta_{s2}, \Theta_{i2}) \right\rangle \quad (2)$$

When the averaging $\langle \dots \rangle$ is performed over samples of a statistically homogeneous domain, the fields will decorrelate except along the “memory line,” determined by the angular relations $\sin(\Theta_{s2}) - \sin(\Theta_{s1}) = \sin(\Theta_{i2}) - \sin(\Theta_{i1})$. This applies for any statistically appropriate source of random reflection in the medium. The effect of the target represents an underlying coherence that will not decorrelate in the same way over the sample space. Here we take care to choose a relevant target with irregularities on the order of the surface perturbations, in part to see whether its effect simply averages out as if it were tantamount to another surface variation. We will proceed by selecting Θ_{i1} , Θ_{i2} , and Θ_{s1} , viewing the results over Θ_{s2} . A major question has been the width of the memory line, i.e. of the region where surface effects may correlate, obscuring the hopefully high ACF value from the target. This relates to our preoccupation with reliability: how decisively (and when) will the target case ACF be larger than that from the surface alone. The ACF/ memory line phenomenon was originally shown to occur for ensembles of spatial samples. Here we must rely more on sampling over frequencies.

Figure 3 shows bistatic ACF bounds computed with frequency averaging but without space shifting. The ACF magnitude is calculated for each surface, with and without buried target; the bounds defined as \pm one standard deviation from ensemble average are determined at each Θ_{s2} . While peaks appear at the memory line angle of -4.5° , they are quite diffuse and ill-defined. In any case, the locus of ACF magnitudes with target present is generally higher than without a target. Next we consider both frequency and spatial averaging. Figure 4 shows quite distinct peaks directly at the

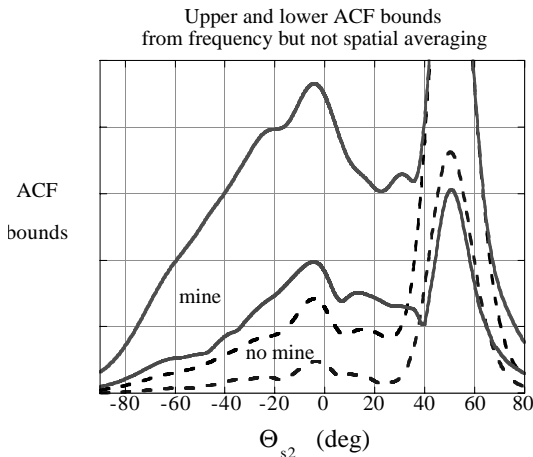


Figure 3. ACF bounds: $\Theta_{i1} = 25^\circ$, $\Theta_{s1} = -25^\circ$, $\Theta_{i2} = 50^\circ$.

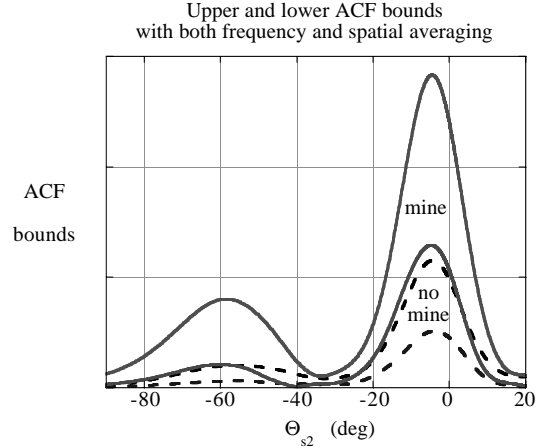


Figure 4. ACF bounds: $\Theta_{i1} = 25^\circ$, $\Theta_{s1} = -25^\circ$, $\Theta_{i2} = 50^\circ$.

memory line angle. Given the range of positions and the frequency band at our disposal, this is about as narrow a memory line as can be achieved. At observation angles Θ_{s2} around -60° , the target would usually though not always be distinguishable. However for Θ_{s2} between about -20° and -55° the distributions overlap badly. Note also that in both target and non-target cases there is a prominent secondary lobe; detectability of the target is distinctly better over these lobes, *including the memory line lobe*. Detection performance is not better in Θ_{s2} regions that show maximum decorrelation behavior ($\Theta_{s2} \sim -30^\circ$). The target seems primarily to intensify the non-zero correlation at the memory line and secondary lobes.

As a second case we reverse the angular selections, with results shown in Figure 5. In this diffuse ACF pattern our angular selection has pushed the memory line to the left beyond real Θ_{s2} . When data from space shifts

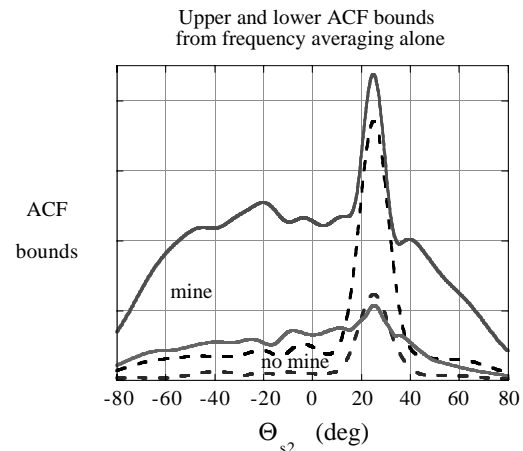


Figure 5. ACF bounds: $\Theta_{i1} = 50^\circ$, $\Theta_{s1} = -50^\circ$, $\Theta_{i2} = 25^\circ$.

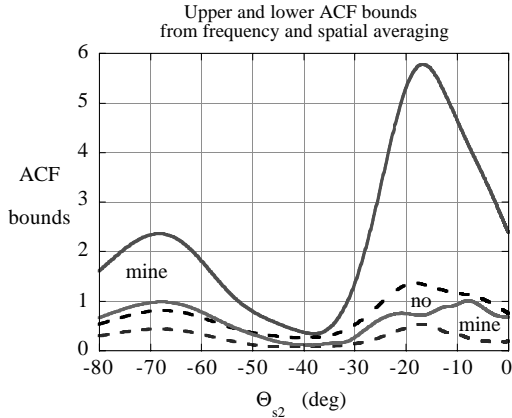


Figure 6. ACF bounds: $\Theta_{i1} = 50^\circ$, $\Theta_{s1} = -50^\circ$, $\Theta_{i2} = 25^\circ$.

is included we obtain Figure 6 where the lobes do not correspond to theoretically identifiable memory effects. Again we note primary and secondary off-specular lobes, with an undesirable amount of overlap between the target and no-target distributions over much of the angular range.

CONCLUSION

The promising new technique of angular correlation function analysis has been applied to simulation

cases involving realistic soil parameters and roughness relative to high resolution GPR wavelengths. A fundamental ACF problem lies in obtaining a profitable ensemble of averaging samples pertaining to a single spot of ground. In general, increasing the sample pool by including overlapping space shifts as well as frequency diversity has improved definition and isolation of the memory line relative to frequency averaging alone. At the same time, this has not improved buried target detection performance in the cases investigated. Ironically, it provided less evidence of the presence of the target in angular zones of maximum noise decorrelation. Interestingly, it seems more to intensify target case ACF response in memory line and secondary lobe regions, relative to the no-target case.

REFERENCES

- [1] K. O'Neill, R.F. Lussky, and K.D. Paulsen, "Scattering from a metallic object embedded near the randomly rough surface of a lossy dielectric," *IEEE Trans. Geosci. Remote Sensing*, vol 34, pp367-376, 1996.
- [2] G. Zhang, L. Tsang, and Y. Kuga, "Studies of the angular correlation function of scattering by random rough surfaces with and without a buried object," *IEEE Trans. Geosci. Remote Sensing*, vol 35, pp444-453, 1997.